A Low-Power Sensitive Integrated Sensor System for Thermal Flow Monitoring

Ruikuan Lu, A. K. M. Arifuzzman, Md Kamal Hossain, Steven Gardner, Sazia A. Eliza, J. Iwan D. Alexander, Yehia Massoud, and Mohammad R. Haider[®]

Abstract-Thermal-based flow monitoring has found widespread applications due to its noncontact measurement, high sensitivity, low flow resistance, miniaturization, ease of integration, and low-power consumption. In this work, a low-cost and affordable inkjet-printed graphene-based thermal sensor is integrated with a low-power CMOS circuit for flow rate monitoring. The custom inkjet-printed sensor consists of a silver nanoparticle interdigitated pattern with a coating of graphene, all printed on a glossy photo-paper substrate. The sensor read-out circuit is an energy-efficient current-starved ring oscillator. The sensor current controls the bias current of a current-starved ring oscillator and modulates the output frequency. A driver circuit then transforms the output to a square wave pulse signal. The scheme is designed and fabricated using the 0.13-\mu m standard CMOS process and occupies an area of 1.5 mm x 1.7 mm. Test results indicate that the prototype ring oscillator circuit consumes 19-90 µW for an oscillation frequency variation of 517 kHz-6.45 MHz. The output frequency variation with sensor current shows linear performance with $R^2 = 0.9966$.

Index Terms—Energy-efficient, graphene, inkjet-printed sensor, read-out circuit, ring oscillator, thermal flow.

I. INTRODUCTION

Recent developments of microfabrication and nanofabrication technologies have led to various physical sensors and sensor electronics integrated on thin films. The miniaturization of sensor devices offers vast opportunities for monitoring and detection applications. Different types of sensor devices have evolved based on material choice and structure. Efforts have also brought sensing and electronics closer to the patient or sensing sites by printing on more adaptable, stretchable, and flexible substrates [1]. These types of sensing systems can be placed on top of human skin or on civil infrastructures for monitoring different physical properties. Liquid flow, fluid dynamics, thermal, gas, and air flow rate measurement devices are reported for a wide variety of industrial applications [2]–[4]. Unlike mechanical deflection schemes, thermal sensors are widely used as flow sensors due to the simple architectures and higher sensitivities.

Low-air-flow sensing systems are crucial for infant cube air-flow monitoring, breathing air-flow detection, and metabolic rate monitoring. Li *et al.* [5] developed a smart catheter flow sensor based on thin film deposition, patterning, and photolithographic techniques for continuous monitoring. However, the sensor sensitivity and the resolution provided in their study still need improvement. In [6], a high-resolution CMOS flow sensor was made by using polysilicon

Manuscript received April 21, 2019; revised June 25, 2019; accepted July 28, 2019. This work was supported in part by the National Science Foundation (NSF) under Award ECCS-1813949 and Award CNS-1645863. (Corresponding author: Mohammad R. Haider.)

R. Lu, M. K. Hossain, S. Gardner, S. A. Eliza, J. I. D. Alexander, and M. R. Haider are with the School of Engineering, University of Alabama at Birmingham, Birmingham, AL 35294 USA (e-mail: lukuan@uab.edu; khossain@uab.edu; stevendg@uab.edu; seliza@uab.edu; ialex@uab.edu; mrhaider@uab.edu).

A. K. M. Arifuzzman is with the College of Engineering, Georgia Institute of Technology, Atlanta, GA 30332 USA (e-mail: arif3@gatech.edu).

Y. Massoud is with the School of Systems and Enterprises, Stevens Institute of Technology, Hoboken, NJ 07030 USA (e-mail: ymassoud@stevens.edu).

Color versions of one or more of the figures in this article are available online at http://ieeexplore.ieee.org.

Digital Object Identifier 10.1109/TVLSI.2019.2935790

microheater and thermopiles array. The reported flow sensor worked with a sensitivity of 0.7 mV/m/s and resolution of 0.001 m/s in the range of flow rate from 0.1 to 3.6 m/s. The reported work shows an improved sensing performance; however, the system consumes a large amount of power, not preferable for a wearable device. In [10], a CMOS time-to-digital converter for a temperature sensor was reported with a power consumption of 400 μ W for 1 kS/s.

1

Recently, graphene-based thermal flow sensors have been designed for improving sensitivity and sensing range [7], [8]. Graphene has a large surface-to-mass ratio and a higher temperature coefficient of resistance than other materials such as platinum, gold, and tungsten. In [9], commercial porous graphene on polyimide film was used to fabricate a flow sensing device. Its reported flow sensor is based on the piezoresistive property that limits its application due to the obstruction in the flow path.

A common engineering challenge is achieving high sensing accuracy at low operating powers with systematic considerations such as sensor cost-effectiveness, user-friendliness, and simplicity. The sensor system presented in this brief is a hybridized system with a low-power integrated circuit (IC) coupled with an inkjet-printed graphene sensor for thermal flow monitoring. The prototype sensor is a low-cost, lightweight, and disposable two-layer sensor printed on glossy photo paper. The read-out circuit comprises a current mirror, a ring oscillator, a level shifter, and a driver network. As the external sensing parameter (i.e., temperature) changes, so does the conductivity of the sensor and the bias current variation of the ring oscillator. The bias current controls the charging and discharging rates of the output capacitors and ultimately changes the output frequency.

The rest of this brief is organized as follows. Section II proposes thermal-based flow monitoring system. Section III provides the custom design and fabrication of the inkjet-printed graphene sensor. Section IV shows the architecture and working principles of the integrated current-starved ring oscillator-based sensor read-out circuit. The test results of the prototype inkjet-printed graphene sensor and the read-out circuit are presented in Section V. Finally, conclusion is drawn in Section VI.

II. THERMAL-BASED FLOW MONITORING SYSTEM

The thermal-based flow monitoring system is shown in Fig. 1. The system consists of a thermal flow sensing device and a sensor read-out IC with the data monitoring unit. The flow sensing device is an inkjet-printed graphene sensor placed inside a cylindrical tube with inlet and outlet openings. The sensor is fabricated in-house by layering silver (Ag) nanoparticle ink and then coating with a second layer of graphene ink to realize the interdigitated electrode pattern on glossy photo paper seen in the upper right of the figure. The conductivity of the sensor changes according to variations of temperature and humidity. Therefore, the air flow sensor can potentially be used in different biomedical applications such as breathing flow monitoring, metabolic observing, and infant cube air flow detection.

The miniaturized energy-efficient CMOS integrated read-out circuit converts the flow sensing signal into a frequency-modulated data signal. The system is comprised of a current mirror, ring oscillator circuit, voltage level shifter amplifier, and a driver circuit. The

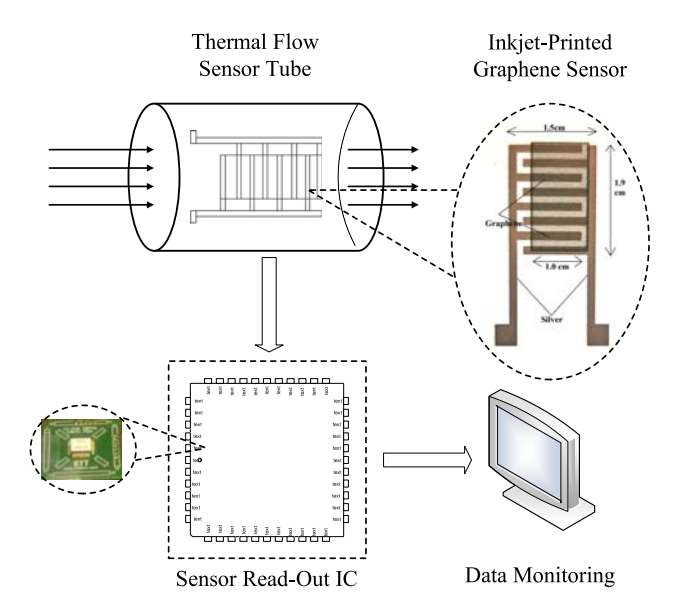


Fig. 1. Schematic overview of a thermal-based flow monitoring system.



Fig. 2. Functional block diagram of thermal flow monitoring system.

functional block diagram of the proposed sensor architecture is shown in Fig. 2. The conductivity change of the sensor creates a bias current variation of the integrated ring oscillator and ultimately modulates the output oscillation frequency. The capacitive inverter-based amplifier circuit shifts the ring oscillator output to a suitable level. At the output of the ring oscillator, the inverter-based driver stage not only drives the external load but also provides the pulse signal. The proposed ring oscillator-based sensor read-out IC is designed and fabricated using $0.13-\mu m$ standard CMOS technology for converting the sensing information into a pulse data signal. All these components are detailed in Sections III and IV.

III. INKJET-PRINTED GRAPHENE SENSOR

Printing electronics on flexible substrates is rapidly developing because of the low-cost fabrication and the ability to design multiplane electronics for functional networks. Standard printed circuit board (PCB) technology works well for most applications due to its high resolution and ease of integration into most modern circuits. The inkjet-printed circuits open the field to more design freedom due to substrate flexibility, ease of editing/reprinting, wide array of ink materials, and low-cost [15]. A printable sensor basically consists of printing materials, circuit structure, and flexible substrates [11].

A. Sensor Material

The printing materials can be divided into three subcategories: conductors, semiconductors, and dielectrics [12], [13]. In this brief, Ag is chosen as the first layer for its high electrical and thermal conductivity, excellent performance on the photo-paper substrate, and high reflectivity. The semiconducting material, graphene, is used as the second (top) layer. Graphene is a single layer of sp²-hybridized carbon atoms, which causes the extraordinarily high thermal and electrical conductivity. It is the thickness of the atom that makes it light, transparent, and flexible. Graphene has high carrier mobility

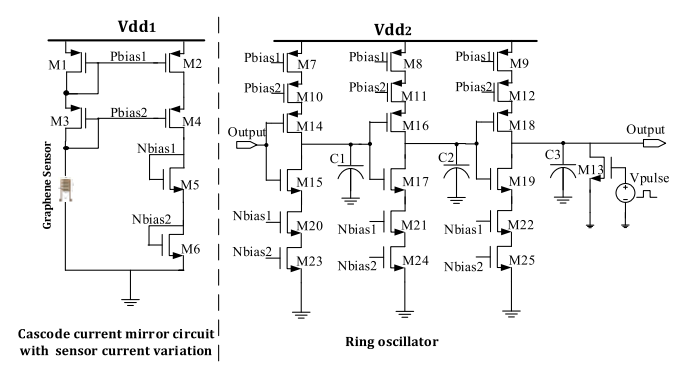


Fig. 3. Circuit schematic of the current-controlled ring oscillator.

 $[10^3 - 10^6 \text{ cm}^2/(\text{V} \times \text{s})]$, density, and conductivity $(10^2 - 10^6 \text{ S/m})$. The unique 2-D structure of graphene has bright prospects in the sensor field. It is very sensitive to the surrounding environment based on its huge surface-to-volume ratio.

B. Sensor Fabrication

In this brief, a commercial PCB layout software application is used to draw the structure of the graphene sensor. A flexible glossy photo paper is used as a sensor substrate in order to achieve lowcost, lightweight, and ease of fabrication goals. A standard desktop Brother printer (MFC-J5910) has been configured by replacing the standard ink contents found in LC75 and LC27 cartridges with a graphene ink in water and a silver nanoparticles ink specific to inkjet printing purchased from Millipore Sigma. The graphene particles are exfoliated graphene flakes of size 80-500 nm. During the curing process, the water evaporates and the flakes dry together at room temperature. It may be annealed in a thermal incubator for performance improvement. The decision to minimize the curing process was to maintain the on-the-go feature desirable for household printed sensors. A prototype inkjet-printed sensor is shown in the upper right corner of Fig. 1 [17]. The sensor's dimension is 1.9 cm × 1.5 cm, the covered graphene dimension is $1.9 \text{ cm} \times 1.0 \text{ cm}$ and the silver linewidth is 1.6 mm. The layer thicknesses of the printed metallic inks are controlled by selecting different printing modes from the Brother printer utility software. This custom setup for inkjet-printing metallic inks obviates the need for expensive nanomaterial inkjetprinters, costing approximately \$50 000 or more.

IV. RING OSCILLATOR-BASED CMOS INTEGRATED READ-OUT CIRCUIT

Our proposed low-power read-out circuit comprises four parts: 1) a self-cascode current mirror to sense the sensor current; 2) a current starved ring oscillator whose output frequency is controlled by the mirror current; 3) an inverter-based capacitive amplifier to shift the output voltage level of the ring oscillator; and 4) an inverter-based driver circuit to drive the pad and external load. A detailed description of the constituent subblocks of the proposed sensor read-out system is provided in Sections IV-A and IV-B.

A. Sensing Mirror and Current Controlled Ring Oscillator

The temperature variation according to air flow is detected by a sensing mirror circuit. Fig. 3 shows the circuit schematic of the proposed current starved ring oscillator. The architecture manifests a three-stage inverter-based ring oscillator, where the bias current of each inverter stage is modulated by the sensor current. Transistors M_{14} – M_{15} , M_{16} – M_{17} , and M_{18} – M_{19} consist of the inverter stages

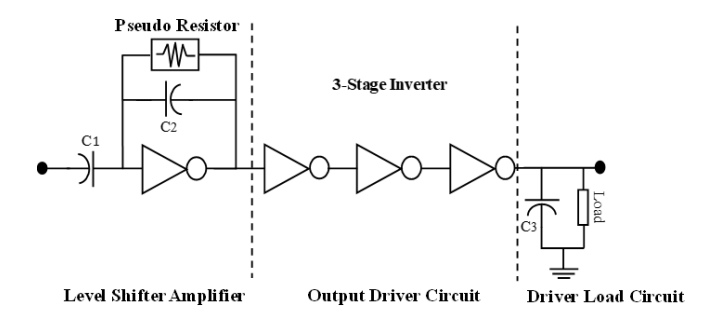


Fig. 4. CMOS inverter-based amplifier and load driver circuit.

and work as the core of the ring oscillator. The bias current of each inverter stage is controlled by a top current mirror (M_1-M_4, M_7-M_{12}) and a bottom current mirror $(M_5-M_6, M_{20}-M_{25})$ for charging and discharging of the output node capacitor of each stage, respectively. The output node capacitor includes the external capacitor $(C_1, C_2, \text{ and } C_3)$ plus the parasitic capacitors from the inverter output stage. The sensor current, modeled by a dc current source in the schematic, is replicated by a cascode current mirror (M_1-M_4) and steered to the top and bottom current mirrors of the inverter stages. Transistor M_{13} is for the initial triggering of the ring oscillator by discharging the output capacitor C_3 . Under the normal operating condition of the ring oscillator, the M_{13} transistor remains off.

The mirror bias current changes with the variation in flow sensor current. The output frequency of the ring oscillator varies with variation of air flow rate since the current of the mirror circuit controls the bias current of the ring oscillator. The oscillation frequency $f_{\rm osc}$ of the proposed ring oscillator depends on the total number of stages m and the time delay τ_d of the oscillator. The oscillation frequency of the ring oscillator is given by

$$f_{\rm osc} = \frac{1}{2m\tau_d}. (1)$$

Here $\tau_d = \tau_{dhl} + \tau_{dlh}$, where τ_{dhl} is defined as the fall time of the ring oscillator output voltage from V_{dd} to $(V_{dd}/2)$ and τ_{dlh} is defined as the rise time of the ring oscillator output voltage from $(V_{dd}/2)$ to V_{dd} .

B. Level Shifter Amplifier and Output Driver

A classic CMOS inverter-based amplifier with capacitive feedback is implemented as a level shifter amplifier as shown in Fig. 4. To bias the input gate terminal and avoid the dc path problem, a pseudoresistor is implemented as a feedback path between the output and input nodes. For the proposed system, a resistance value of 50 M Ω is realized by using a diode-connected MOS-based pseudoresistance with device aspect ratio of $(W/L) = (250 \ \mu\text{m}/250 \ \text{nm})$. The output signal of the amplifier circuit is fed to the driver block to drive the external load. The driver circuit comprises three-stage cascaded inverter blocks. The size of each stage CMOS inverter is doubled in the following stage. This driver circuit is designed to drive a load capacitor C_3 of 30 pF and a resistance of 50 Ω as the load block of the driver unit as shown in Fig. 4.

V. TEST RESULTS AND DISCUSSION

The prototype sensor was placed inside the cylindrical tube as shown in Fig. 5. The sensor was attached to the interior wall of the cylinder with the working layer of the sensor exposed to internal flow sensing. In this test, the thermal air variation was produced by human exhalation and inhalation. Two copper wires were connected

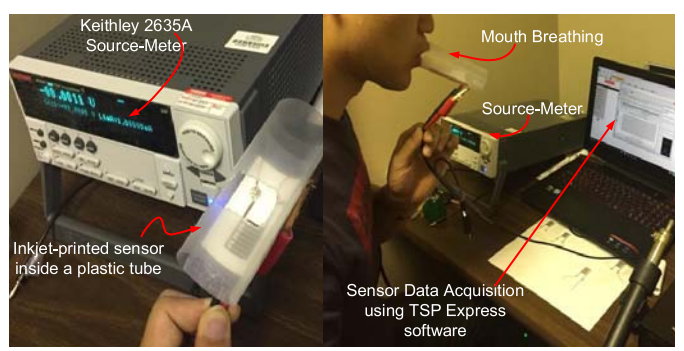


Fig. 5. Test setup of the sensor tube for breathing flow monitoring.

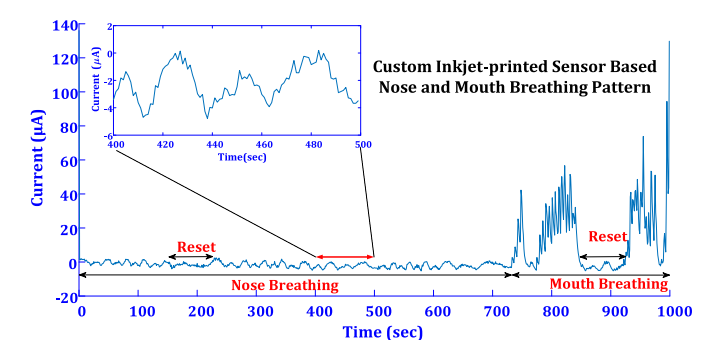


Fig. 6. Nose and mouth breathing patterns observed by graphene-based inkjet-printed sensor.

to the terminals of the sensor to collect the information so that the sensitivity and performance of the graphene sensor may be examined. A high-precision Keithley 2635A meter was used to observe the sensor current variations with changing respiratory rates during the test phase. For the test, 20-V dc was used as the supply source at room temperature of 20 °C. Fig. 6 shows the variation of graphene sensor conductivity from human breathing rate. Both the nose and mouth breathing patterns were measured by the proposed inkjet-printed sensor. During the test phase, the sensor had been reset before every test by an air heating gun. After reset, the prototype sensors returned to normal operating mode. Fig. 6 also shows that the value of sensing current was higher from the mouth breathing than from the nose breathing, which can be explained by the higher air flow rate. Based on the results, the low-cost inkjet-printed sensor accurately senses thermal air flow for a respectable amount of time (hundreds of seconds) [17].

A. Test Results of Sensor Read-Out IC

The proposed fabricated sensor read-out chip was wire-bonded in a 44-pin OCP-LQFP-44A package for minimum package parasitic from the bond wires and the package pins. The custom packaged chip was then solder-mounted on an FR4 PCB and the prototype chip performance was tested using a laboratory bench-top setup as shown in Fig. 7. A wrist strap connected to the supply ground was used to discharge the human body and prevent any electrostatic discharge (ESD) damage of the chip. Two different dc supply voltages (0.8 and 0.4 V) were used for the ring oscillator and the driver circuit, respectively. To start the oscillation of the ring oscillator, transistor M_{13} was triggered by applying a square pulse signal of 500 mV (peak to peak). To monitor the oscillation frequency of the ring oscillator pulse signal, an oscilloscope (MSO-X 3024A) probe was connected at the output of the prototype ring oscillator.

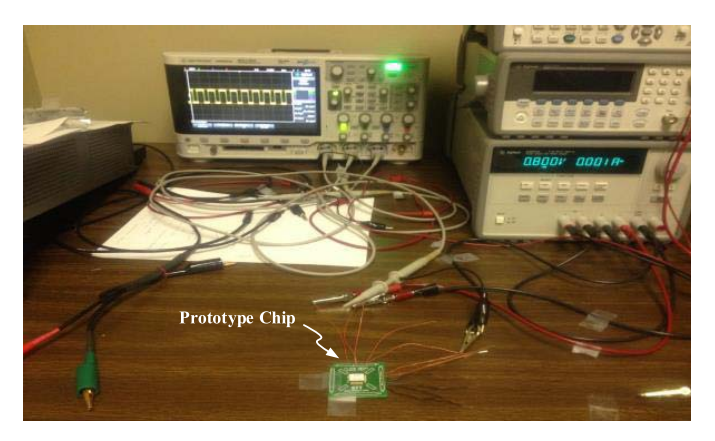


Fig. 7. Test setup of the ring oscillator-based sensor read-out circuit.

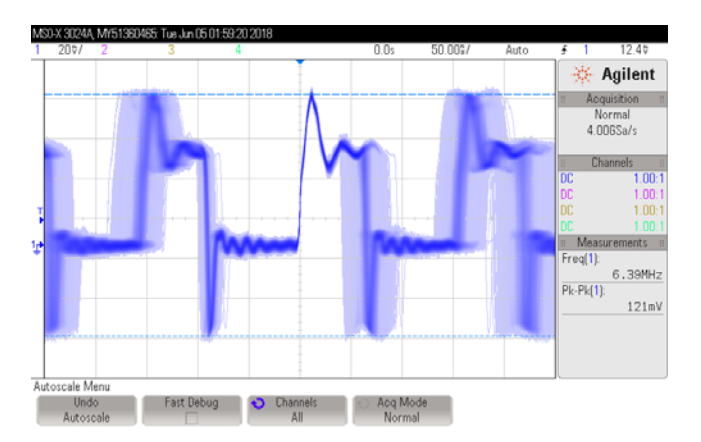


Fig. 8. Test result of output pulses for a bias current variation of 200 nA.

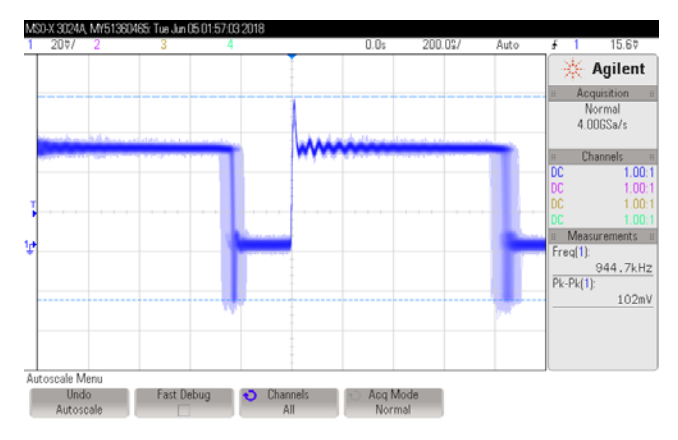


Fig. 9. Test result of output pulses for a bias current variation of 18 μ A.

To verify the performance of the sensor read-out circuit, a current source was used to supply the bias current in the current mirror-based ring oscillator. In this test, the Keithley 2635A source-meter was used as a current source. The blue trace in Fig. 8 represents the ring oscillator output pulses corresponding to the bias current variation of 200 nA. The bias current is varied from 50 nA to 35.2 μ A. In order to verify the sensitivity of the sensor read-out circuit, the supply current was varied gradually while observing the ring oscillator output frequency pulses. Fig. 9 shows the output pulses of the ring oscillator corresponding to the bias current variation of 18 μ A.

Fig. 10 shows the ring oscillator power consumption corresponding to the variation of sensor bias current from the source-meter. The variation of sensor read-out IC output covers a wide linear range with the changing sensor bias current. As seen from Fig. 10, the power

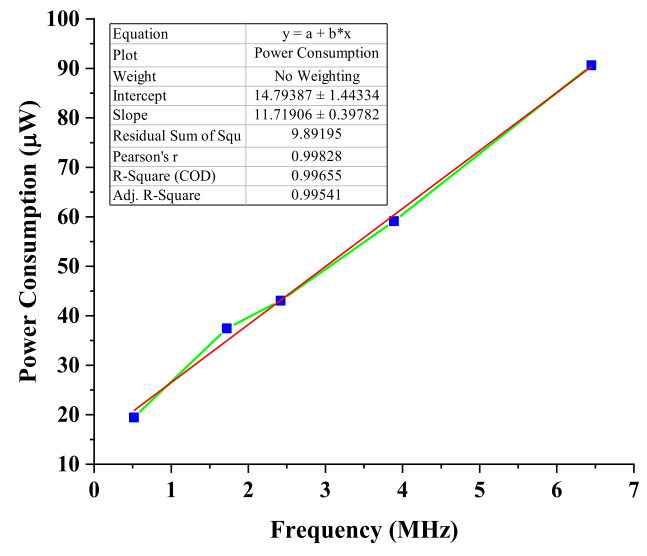


Fig. 10. Power consumption by sensor read-out IC with frequency variation.

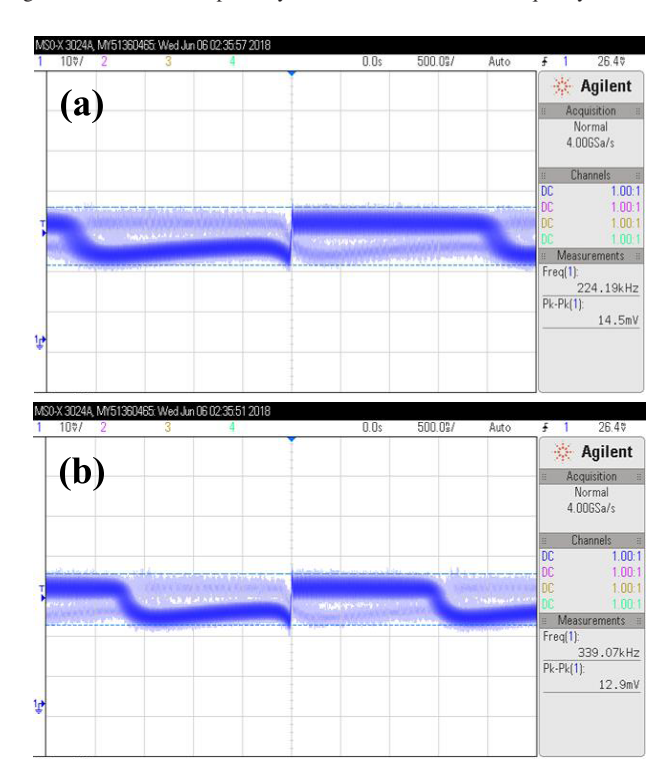


Fig. 11. Test results of sensor with read-out IC at (a) maximum inhale and (b) maximum exhale conditions.

consumption variations with the ring oscillator frequency (corresponding to the sensor current) follow a linear variation with linearity measure $R^2 = 0.9966$. The variation of IC power consumption and the linear performance for current to frequency conversion with high linearity property indicate the effectiveness of the proposed scheme for energy-efficient portable device applications.

B. Test Results of Read-Out IC With Graphene Sensor

In this test, a 9 V dc supply was used to energize the prototype graphene sensor, and the output of the sensor was connected to the custom read-out IC's input bias current pin. The output frequency of the sensor read-out IC changed from 224 to 339 kHz corresponding to the maximum inhale and exhale, respectively. The experimental results at two different breathing conditions are shown in Fig. 11.

VI. CONCLUSION

A low-cost disposable graphene nanoparticle-based sensor with an energy-efficient sensor read-out IC is demonstrated in this brief. The sensor is fabricated on glossy photo paper using a standard office inkjet-printer while the sensor read-out IC is fabricated using 0.13-µm standard CMOS technology. The test results indicate the prototype sensor with the integrated sensor read-out IC can achieve higher sensitivity performance for measuring the low thermal air flow from human breathing cycles. The proposed air flow sensor can recognize short-term breathing patterns and the IC is reliable for long term operation. The current starved ring oscillator-based sensor read-out circuit architecture and subthreshold region operation make the design ideal for low-power applications. The test results show the power consumption of the prototype sensor read-out IC to be in the microwatt range. The IC power consumption is 19-90 μ W corresponding to the output frequency pulses of 517 kHz to 6.45 MHz, respectively. The fabricated IC also shows a high dynamic range for sensor current variation and linear performance for sensing current to frequency conversion with a linearity measure $R^2 = 0.9966.$

ACKNOWLEDGMENT

The authors would like to thank MOSIS (www.mosis.com) for fabricating the integrated circuit.

REFERENCES

- T. Vuorinen, J. Niittynen, T. Kankkunen, T. M. Kraft, and M. Mäntysalo, "Inkjet-printed graphene/PEDOT:PSS temperature sensors on a skinconformable polyurethane substrate," Sci. Rep., vol. 6, Oct. 2016, Art. no. 035289.
- [2] A. K. M. Arifuzzman, M. R. Haider, and D. B. Allison, "A low-power thermal-based sensor system for low air flow detection," *Analog Integr. Circuits Signal Process.*, vol. 89, no. 2, pp. 425–436, 2016.
- [3] F. Wenig, C. Heschl, T. Glatzl, and T. Sauter, "Numerical and experimental characterization of a novel low-cost thermal air flow sensor," in *Proc. 43rd Annu. Conf. IEEE Ind. Electron. Soc.*, Beijing, China, Oct./Nov. 2017, pp. 3633–3637.

- [4] Y. Cao, Z. Xie, and C. Hou, "Flow rate measurement system using thermal air flow sensor," in *Proc. 9th Int. Conf. Electron. Meas. Instrum.*, Beijing, China, Apr. 2009, pp. 2885–2889.
- [5] C. Li, P.-M. Wu, Z. Wu, C. H. Ahn, J. A. Hartings, and R. K. Narayan, "Smart catheter flow sensor for continuous regional cerebral blood flow monitoring," in *Proc. IEEE SENSORS*, Limerick, Ireland, Oct. 2011, pp. 1417–1420.
- [6] L.-C. Chang, Y.-W. Deng, D. Lee, and C.-S. Chen, "Development of a high resolution CMOS flow sensor," in *Proc. 1st IEEE Int. Conf. Nano/Micro Eng. Mol. Syst.*, Zhuhai, China, Jan. 2006, pp. 890–895.
- [7] H. Al-Mumen, F. Rao, L. Dong, and W. Li, "Thermo-flow and temperature sensing behaviour of graphene based on surface heat convection," *IET Micro Nano Lett.*, vol. 8, no. 10, pp. 681–685, Oct. 2013.
- [8] Z. Liu and F. Xu, "Miniature sensor based on fiber-graphene-integrated NEMS," in *Proc. 16th Int. Conf. Opt. Commun. Netw.*, Wuzhen, China, Aug. 2017, pp. 1–2.
- [9] M. Marengo, G. Marinaro, and J. Kosel, "Flexible temperature and flow sensor from laser-induced graphene," in *Proc. IEEE SENSORS*, Glasgow, U.K., Nov. 2017, pp. 1–3.
- [10] C.-C. Chen, A.-W. Liu, Y.-C. Chang, and P. Chen, "An accurate CMOS time-to-digital-converter-based smart temperature sensor with negative thermal coefficient," in *Proc. IEEE SENSORS*, Irvine, CA, USA, Oct./Nov. 2005, pp. 1–4.
- [11] A. Gordon, G. W. Roberts, and C. J. Fayomi, "Low-cost trimmable manufacturing methods for printable electronics," in *Proc. IEEE Int. Symp. Circuits Syst.*, Montreal, QC, Canada, May 2016, pp. 870–873.
- [12] W. Y. Chang, T. H. Fang, H. J. Lin, Y. T. Shen, and Y. C. Lin, "A large area flexible array sensors using screen printing technology," *J. Display Technol.*, vol. 5, no. 6, pp. 178–183, Jun. 2009.
- [13] H. Jiang, S. Arabi, H. Shahbazbegian, J. N. Patel, and B. Kaminska, "Inkjet printed optically variable devices on a polymer substrate patterned with nanopillar array structural pixels," in *Proc. IEEE 15th Int. Conf. Nanotechnol.*, Rome, Italy, Jul. 2015, pp. 1394–1397.
- [14] V. Correia et al., "Design and fabrication of multilayer inkjet-printed passive components for printed electronics circuit development," J. Manuf. Processes, vol. 31, pp. 364–371, Jan. 2018.
- [15] S. Mandal, G. Purohit, and M. Katiyar, "Inkjet printed organic thin film transistors: Achievements and challenges," *Mater. Sci. Forum*, vol. 736, pp. 250–274, Jan. 2018.
- [16] M. Singh, H. M. Haverinen, P. Dhagat, and G. E. Jabbour, *Inkjet Printing—Process and its Applications*, vol. 2. Weinheim, Germany: Wiley, pp. 673–685.
- [17] R. Lu, M. R. Haider, S. Gardner, J. I. D. Alexander, and Y. Massoud, "A paper-based inkjet-printed graphene sensor for breathing-flow monitoring," *IEEE Sensors Lett.*, vol. 3, no. 2, Feb. 2019, Art. no. 6000104.